Ocean Engineering 173 (2019) 556–570

Contents lists available at ScienceDirect

Ocean Engineering

journal homepage: www.elsevier.com/locate/oceaneng

Modeling dynamic responses of heterogeneous seabed with embedded pipeline through multiresolution random field and coupled hydromechanical simulations

Zhengshou Lai[c], Qiushi Chen[a,*], Chaofeng Wang[d], Xianglian Zhou[b]

[a] Glenn Department of Civil Engineering, Clemson University, Clemson, SC, 29634, USA
[b] Centre for Marine Geotechnical Engineering, Shanghai Jiao Tong University, Shanghai, 200240, China
[c] School of Intelligent Systems Engineering, Sun Yat-sen University, Guangzhou, 510275, China
[d] The Computational Modeling and Simulation Center, University of California - Berkeley, Berkeley, CA, 94720, USA

ARTICLE INFO

Keywords:
Hydromechanical coupling
Random field models
Porous seabed
Spatial variability
Wave-seabed-pipeline interaction

ABSTRACT

In this work, novel multiresolution random field models are integrated with coupled hydromechanical finite element simulations to model dynamic responses of heterogeneous seabed with embedded pipeline subjected to nonlinear wave-induced loadings. The heterogeneous properties of the seabed are characterized and modeled as spatially correlated random variables. A conditional sequential simulation technique is implemented and multiresolution random field realizations of heterogeneous properties are generated. The effects of spatially correlated seabed properties on the characteristic hydromechanical responses are analyzed in details through validated hydromechanical finite element simulations. Statistics and associated uncertainties of system response are obtained with recourse to Monte Carlo simulations. The relations between the inherent heterogeneities and uncertainties in the system responses are derived. Findings of this study are shown to have important implications for probabilistic engineering designs.

1. Introduction

Design of submarine infrastructure, such as embedded pipelines, require the understanding and the ability to predict the behavior of submarine infrastructure and the surrounding seabed subjected to wave-induced loadings. The influence of the wave loading on embedded pipelines is mainly characterized by two aspects. First, the dynamic wave loading induces oscillatory excess pore pressure within the porous seabed, which directly results in oscillatory stresses and deformations within the embedded pipeline. Second, the excess pore pressure built-up during the propagation of dynamic waves may lead to transient liquefaction of the seabed soil (Tsui and Helfrich, 1983; Ye, 2012), which causes the loss of loading bearing capacity of the soil around the pipeline. Therefore, when it comes for an engineer to design the pipeline, it is of particular importance to predict the wave-induced dynamic responses and quantities of interest such as the excess pore pressure, the stress, and deformation in the pipeline and the extent of liquefaction.

Modeling the wave-induced hydromechanical responses of the seabed-pipeline system necessitates the integration of multiple models that account for the nonlinear wave-induced loading, the inherent heterogeneities of the seabed, the interaction between fluid diffusion and solid deformation within the porous seabed and the stresses and deformations within the pipeline. In simplified models, the pipeline was treated as a rigid body or elastic solid while the surrounding seabed was assumed to be a homogeneous, isotropic and elastic media (Cheng and Liu, 1986; Magda, 1997; Jeng and Cheng, 2000; Jeng et al., 2001; Zhao et al., 2016a). However, natural seabed sediments are usually formed from a vertical consolidation process under overburden pressure coming from self-weight and wave loading. This process may result in significant cross-anisotropy and depth-dependency in seabed properties. For example, the permeability of seabed is found to decrease with depth as a result of decreasing porosity of the seabed due to the consolidation process (Seymour et al., 1996).

The seabed cross-anisotropy can be described by assuming different material properties along the vertical and horizontal directions (Gatmiri, 1992; Jeng, 1997; Kitano and Mase, 1999; Jeng and Lin, 1999, 2000a; Wang et al., 2000; Zhou et al., 2014; Zhao et al., 2016b). Some early work used the finite element method or developed analytical solutions to study the effects of cross-anisotropy on the wave-

* Corresponding author.
E-mail address: qiushi@clemson.edu (Q. Chen).

https://doi.org/10.1016/j.oceaneng.2019.01.015
Received 8 March 2017; Received in revised form 26 August 2018; Accepted 4 January 2019

induced seabed response (Gatmiri, 1992; Jeng, 1997; Kitano and Mase, 1999; Jeng and Lin, 2000a). Later, the wave-induced soil response around a buried pipeline was investigated in (Jeng and Lin, 1999; Wang et al., 2000) using two-dimensional finite element models. The wave-seabed-pipeline framework is then extended to a dynamic hydro-mechanical problem by Zhou et al. (2014) with the consideration of soil skeleton accelerations, and Zhao et al. (2016b) further elaborated this framework by incorporating an elasto-plastic seabed model. Among these works on studying wave-seabed-pipeline behavior, it is found that the effect of anisotropic soil behavior was more apparent near the bottom of the pipe than at the top of the pipe (Wang et al., 2000), and liquefaction was more likely to occur in anisotropic soils than in isotropic soils, especially in the vicinity of a pipeline (Zhao et al., 2016b).

To consider the depth-dependent seabed parameters, one approach is to divide the seabed into a number of sub-layers with finite thickness and assign uniform permeability, porosity and shear modulus for each sub-layer (Hsu et al., 1995; Zhou et al., 2011, 2013; Ulker, 2012). Another approach is to describe the seabed parameters using continuous depth-dependent functions (Jeng and Seymour, 1997; Jeng and Lin, 2000b; Jeng, 2001; Gao et al., 2003). For instance, four different types of analytical function for depth-dependent hydraulic conductivity were proposed in (Jeng and Seymour, 1997). The effects of depth-dependent seabed parameters on the wave-seabed-pipeline behavior were analyzed through analytical and numerical models in recent works (Zhou et al., 2011, 2013; Jeng and Lin, 2000b; Jeng, 2001; Gao et al., 2003).

In addition to the cross-anisotropy and depth-dependency characteristics of the seabed, inherent heterogeneities also exist in the seabed due to its deposition processes (Goff et al., 2004, 2008; Veloso et al., 2016). The previously mentioned models for anisotropy or depth-dependency may not necessarily capture the effects of seabed heterogeneities and the modeling results are only deterministic in nature. Though without consideration of any submarine structure, the work of Zhang et al. (2016) is among the first efforts to consider the omnidirectional spatial variability of the seabed, where the soil properties in the field were considered to consist of two parts, a trend component and a residual term that exhibits spatial correlation. Random fields of seabed properties were generated and coupled with finite element models to simulate responses of the seabed. In a recent work by Peng et al. (2017), the effects of cross-correlation of the seabed soil properties on wave-induced oscillatory seabed response were studied and it was found that multiple correlated random properties would lead to greater uncertainties in the excess pore pressure. While the effects of spatial variability on seabed response have been studied previously, its effects on the embedded pipeline and implications on probabilistic engineering design have not been addressed yet.

In this work, a framework accounting for the inherent heterogeneities of a porous seabed and the coupled hydromechanical behavior is presented to model the wave-induced dynamic responses of a heterogeneous seabed-pipeline system. Details of the dynamic hydro-mechanical problem formulation are presented in Section 2. A multi-resolution random field model is developed in Section 3 to characterize and generate spatially correlated, heterogeneous and anisotropic seabed fields, which will be coupled and implemented into a multi-physics finite element model (Section 4). In Section 5, Monte Carlo simulations will be performed to investigate the impact of heterogeneous seabed on the hydromechanical responses of the system and the implications on probabilistic engineering design.

1.1. Formulation of the dynamic hydromechanical coupled problem

The problem considered in this work is a dynamic hydromechanical problem, where the wave propagates over a heterogeneous porous seabed with an embedded submarine pipeline (Fig. 1). The problem is treated as a plane strain problem, where the dimension of the pipeline in the y-direction is much larger and its deformation along y-direction is neglected. The seabed is modeled as a poroelastic material while the embedded pipeline is modeled as an elastic solid.

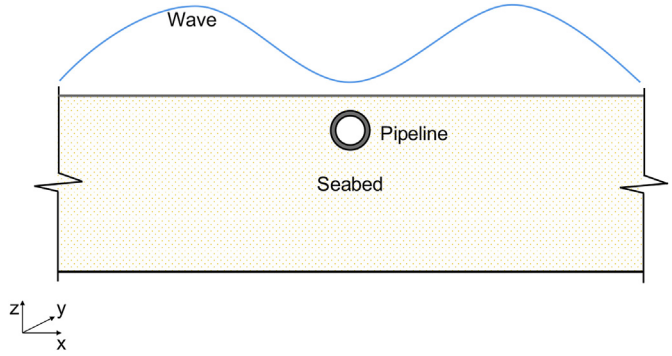

Fig. 1. A schematic diagram of the dynamic hydromechanical coupled problem.

2.1. Balance laws

The balance laws of porous seabed consist of two sets of partial differential equations (PDEs), i.e., the balance of mass equation and the balance of linear momentum equation. In deriving the balance of mass equation, both the compressibility of the pore fluid and the degree of saturation of the porous seabed are accounted for. The final form of the balance of mass equation is written as

$$\nabla\cdot(\boldsymbol{K}\cdot\nabla p) - \phi_f\rho_f g\beta\frac{\partial p}{\partial t} + \rho_f\nabla\cdot(\boldsymbol{K}\cdot\boldsymbol{a}) - \rho_f g\nabla\cdot\boldsymbol{v} = 0 \tag{1}$$

where $\boldsymbol{K}$ is the hydraulic conductivity tensor of the seabed; p is the excess pore pressure; ϕ_s and ϕ_f are the volume fractions of the solid skeleton and void (including gas and fluid), respectively; ρ_f is the intrinsic mass density of the fluid; g is the gravitational acceleration; $\boldsymbol{a}$ and $\boldsymbol{v}$ are the acceleration and velocity, respectively. The parameter β accounts for both the compressibility of the pore fluid and the degree of saturation of the porous seabed and is given as

$$\beta = \frac{1}{k_f} + \frac{1 - S_r}{p_{f0}} \tag{2}$$

where S_r is the degree of saturation; k_f is the bulk modulus of the fluid and p_{f0} is the static pore pressure.

The balance of linear momentum equation of the porous seabed is given as

$$\nabla\cdot\boldsymbol{\sigma}' - \nabla p + \rho\boldsymbol{b} = \rho\boldsymbol{a} \tag{3}$$

where $\boldsymbol{\sigma}'$ is the effective stress of the porous seabed; p is the excess pore pressure; $\boldsymbol{b}$ is the body force; $\rho = \phi_s\rho_s + \phi_f\rho_f$ is the equivalent density of the porous seabed with ρ_s and ρ_f being the intrinsic mass density of the fluid and solid, respectively.

For the embedded pipeline, the balance of linear momentum equation is given as

$$\nabla\cdot\boldsymbol{\sigma} + \rho_p\boldsymbol{b} = \rho_p\boldsymbol{a} \tag{4}$$

where $\boldsymbol{\sigma}$ is the total stress of the pipeline and for single phase (solid) material, $\boldsymbol{\sigma} = \boldsymbol{\sigma}'$ with $\boldsymbol{\sigma}'$ being the effective stress; ρ_p is the mass density of the pipeline. Perfect bonding is assumed between the pipeline and seabed.

2.2. Constitutive relations

Elastic constitutive relations are assumed for both the seabed solid skeleton and the pipeline. Based on the generalized Hooke's law

$$\boldsymbol{\sigma}' = \boldsymbol{c}\cdot\boldsymbol{\varepsilon} \tag{5}$$

where, for the plane strain problem considered, the effective stress in Voigt notation is given as $\boldsymbol{\sigma}' = \{\sigma_{xx}, \sigma_{zz}, \sigma_{xz}\}^T$ and the strain is given as

$\boldsymbol{\varepsilon} = \{\varepsilon_{xx}, \varepsilon_{zz}, \varepsilon_{xz}\}^T$. It should be emphasized that, for the porous seabed, $\boldsymbol{\sigma}' = \boldsymbol{\sigma} - p\boldsymbol{\delta}$, and for the solid pipeline, $\boldsymbol{\sigma}' = \boldsymbol{\sigma}$. $\boldsymbol{c}$ is the elastic modulus given as

$$\boldsymbol{c}_{s,p} = \frac{2G_{s,p}}{(1-2\nu_{s,p})}\begin{bmatrix} 1-\nu_{s,p} & \nu_{s,p} & 0 \\ \nu_{s,p} & 1-\nu_{s,p} & 0 \\ 0 & 0 & 1-2\nu_{s,p} \end{bmatrix} \tag{6}$$

where G is the shear modulus and ν is the Poisson's ratio; the subscript 's' corresponds to the seabed skeleton and 'p' corresponds to the pipeline. While elastic constitutive relations assumed for its simplicity and computational efficiency, their limitations should also be noted. The elastic models cannot capture permanent deformations of the marine soils or the pipeline. More advanced elastoplasticity model would need to be implemented for this purpose, which typically involves additional model parameters that need to be calibrated and is generally computational expensive.

2.3. Wave-induced nonlinear loading on the seabed

In general, the wave characteristic will be changed due to the interaction between the wave and the seabed. For deeper water, however, such interaction can be neglected. In this work, the change of wave characteristics is assumed to be negligible. Therefore, the vertical effective stress σ'_{zz} and the shear stress σ'_{zx} induced by the wave on the seabed boundary can be neglected (Yamamoto and Suzuki, 1980). The wave-induced loading is applied on the seabed boundary as a time-varying pore pressure function $p_b(t)$ with t being time as follows

$$\sigma'_{zz} = \sigma'_{zx} = 0, \quad p = p_b(t) \quad \text{at } z = 0 \tag{7}$$

The cyclic variation of pore pressure is estimated by an analytic formulation of wave pressure on the seabed surface (Zhou et al., 2013). Generally, Stokes wave theory is of direct practical use for waves on intermediate and deep water. According to the first-order Stokes wave, the dynamic variation of wave pressure $p_b(t)$ is (Zhou et al., 2013)

$$p_b(t) = p_0 \cos\left(2\pi\frac{x}{L} - \omega t\right) = \frac{1}{2}\rho_f g \cosh^{-1}(2\pi d/L)\cos\left(2\pi\frac{x}{L} - \omega t\right) \tag{8}$$

where d is the water depth; L and H are the wavelength and height, respectively; ω is the angular frequency of the wave; and p_0 denotes the amplitude of the wave pressure at the seabed surface.

2.4. Transient liquefaction criteria

Dynamic loading of ocean wave could induce oscillatory excess pore pressure within the porous seabed, which leads to oscillatory effective stress and liquefaction of the seabed. When the marine soil liquefies, it loses its load bearing capacity and behaves as a viscous liquid, potentially causing damages to the embedded infrastructure. Therefore, liquefaction of seabed under dynamic wave loading is an important aspect that will be analyzed. In this work, the transient liquefaction criterion is adopted as follows (Zen and Yamazaki, 1990a, 1990b)

$$-(\gamma_s - \gamma_f)z + p_b(t) - p \le 0 \tag{9}$$

where $p_b(t)$ is the dynamic wave pressure defined in Eq. (8) and p is the excess pore pressure in the seabed. This criterion is simple in form and has a direct physical interpretation that the seabed will liquefy if the upward seepage force can overcome the effective self-weight of the overburdened soil.

To quantify and compare the extent of liquefaction, previous works have recourse to the maximum depth of liquefaction (Jeng and Cheng, 2000; Zhou et al., 2013). However, the maximum depth of liquefaction gives only limited information regarding the extent of liquefaction. Moreover, when heterogeneity of seabed is accounted for, the liquefaction area boundary profile can be tortuous. In this work, a new parameter indicating the area ratio of liquefaction is proposed to quantify and compare the liquefaction extent. The parameter is defined as the ratio of the area of liquefaction to the total area of the domain of influence, which is taken as five times the diameter of the pipeline and is illustrated in Fig. 2. The choice of five times is based on a preliminary investigation of the excess pore pressure built-up around the pipeline when the wave propagates and it was found that the domain of five times the diameter approximately covers the area of the most excess pore pressure built-up, especially in the vertical direction.

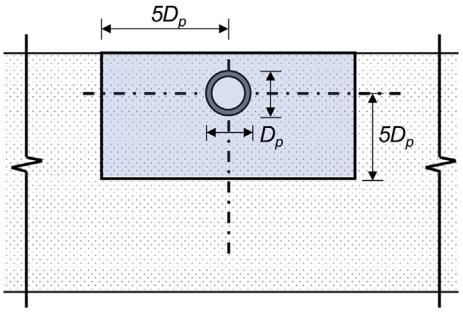

Fig. 2. The schematic diagram of the domain of influence (colored in light blue) of seabed soil liquefaction. (For interpretation of the references to color in this figure legend, the reader is referred to the Web version of this article.)

3. Multiresolution random field characterization of the heterogeneous seabed

Inherent heterogeneities, i.e., those resulting from fluctuations in material properties such as hydraulic conductivity or shear modulus, exist in natural geological materials, including the marine soil. In this section, a multiresolution random field is presented to characterize and model the inherent heterogeneities in the porous seabed. The random field model will then be coupled with multiphysics finite element model (Section 4) and Monte Carlo simulations to analyze the impact of inherent heterogeneities on the seabed-pipeline system response.

3.1. Characterization of anisotropic spatial dependency

Seabed properties generally exhibit variation with space and such variation is spatially correlated or dependent, which is typically attributed to the deposition process of the seabed. In this study, the spatial dependency is described using a form of covariance known as the semivariogram, $\gamma(\boldsymbol{h})$, which is equal to half the variance of the difference of two random variables separated by a vector distance $\boldsymbol{h}$

$$\gamma(\boldsymbol{h}) = \frac{1}{2}\mathrm{Var}[Z(\boldsymbol{x}) - Z(\boldsymbol{x}+\boldsymbol{h})] \tag{10}$$

where $Z(\boldsymbol{x})$ is a Gaussian random variable at location $\boldsymbol{x}$ with $\boldsymbol{x} = \{u, w\}$ being the location vector. The vector $\boldsymbol{h}$ accounts for both the separation distance and the orientation of two points in the random field. In the actual implementation, a simplified scalar measure h is typically defined

$$h = \sqrt{\left(\frac{h_x}{\theta_x}\right)^2 + \left(\frac{h_z}{\theta_z}\right)^2} \tag{11}$$

where h_x and h_z are the scalar component of the vector $\boldsymbol{h}$ along the field's principal axes x and z, respectively; scalar quantities θ_x and θ_z specify how quickly spatial dependence decreases along those axes. By skewing the ratio of θ_x and θ_z, anisotropic random fields can be generated, which is particularly useful for modeling heterogeneous seabed properties that typically exhibit anisotropy as will be shown in the example section.

In practice, various analytical semivariogram models and their linear combinations are typically fitted to an empirical semivariogram that is calculated from field data. Examples of commonly used

analytical semivariogram models include the nugget effect model, the linear model, the spherical model, the exponential model and the Gaussian model (Goovaerts, 1997). The specific model form can be inferred from available field data or assumed based on expert knowledge. For marine deposit, studies and data on the spatial variability of its properties are relatively limited. In (Valdez-Llamas et al., 2003), the spatial variability of the cohesive soft soil thickness and the water content of a marine soil are found to be exponential. In several other studies that consider the randomness of marine soils, the exponential correlation structure is also used (e.g. (Zhang et al., 2016; Peng et al., 2017; Lloret-Cabot et al., 2014),). While there lacks sufficient data or clear evidence pointing to a specific spatial structure, an exponential model is assumed in this work to illustrate the proposed framework. It should be noted that whenever there are sufficient field data, the specific spatial correlation structure can always be inferred. The expression of the adopted exponential model is

$$\gamma(h) = 1 - \exp(-h) \tag{12}$$

3.2. Multiresolution random field and conditional simulation algorithm

Given the spatial correlation model and a specified or inferred probability distribution function for the random variable, a conditional sequential simulation algorithm is implemented in this work to generate random field realizations of material properties. This algorithm is particularly valuable for the multiresolution random field utilized in this study, where a higher resolution field is desired around the area adjacent to the embedded pipeline (see illustration in Fig. 3). With this algorithm, one can simply add additional random field data points wherever and whenever is necessary during the simulation process, conditional upon all previously simulated data and as the need arises. An additional advantage of this algorithm is that it allows real data points to be incorporated and preserved in the generated random field (e.g. (Chen et al., 2015; Liu et al., 2017),).

Denote $\boldsymbol{Z}_p$ as a vector of all known and previously simulated points in the random field and denote Z_n as the next point to be simulated, the sequential simulation process can be illustrated by the joint distribution (Chen et al., 2012)

$$\begin{bmatrix} Z_n \\ \mathbf{Z}_p \end{bmatrix} \sim N\left(\boldsymbol{\mu}, \begin{bmatrix} \sigma_n^2 & \boldsymbol{\Sigma}_{np} \\ \boldsymbol{\Sigma}_{pn} & \boldsymbol{\Sigma}_{pp} \end{bmatrix}\right) \tag{13}$$

where $\sim N(\boldsymbol{\mu}, \boldsymbol{\Sigma})$ denotes the vector of random variables following a joint normal distribution with the mean vector $\boldsymbol{\mu}$ and the covariance matrix $\boldsymbol{\Sigma}$; σ_n^2 is the prior variance of the next simulated point; $\boldsymbol{\Sigma}_{np}$, $\boldsymbol{\Sigma}_{pn}$ and $\boldsymbol{\Sigma}_{pp}$ are the covariance matrices, where the subscripts 'n' and 'p' represent 'next' (as in next point to be simulated) and 'previous' (as in all previously simulated points), respectively. The covariance matrices are obtained by

$$\mathrm{COV}[Z_i, Z_j] = \rho_{ij} \cdot \sigma_i \cdot \sigma_j \tag{14}$$

where ρ_{ij} is the correlation between random variables Z_i and Z_j with standard deviations of σ_i and σ_j, respectively. The correlation ρ is related to the semivariogram defined in Eq. (10) through

$$\rho(h) = 1 - \gamma(h) \tag{15}$$

where h is the scalar distance given in Eq. (11).

Using the joint distribution Eq. (13), the distribution of Z_n conditional upon all previously simulated data is given by a univariate normal distribution with the updated mean and variance as (Chen et al., 2012)

$$(Z_n | \boldsymbol{Z}_p = \boldsymbol{z}) \sim N(\boldsymbol{\Sigma}_{np} \cdot \boldsymbol{\Sigma}_{pp}^{-1} \cdot \boldsymbol{z},\ \sigma_n^2 - \boldsymbol{\Sigma}_{np} \cdot \boldsymbol{\Sigma}_{pp}^{-1} \cdot \boldsymbol{\Sigma}_{pn}) \tag{16}$$

where the lowercase $\boldsymbol{z}$ represents the vector of simulated values; other terms have been defined after Eq. (13).

The conditional simulation starts with a single realization of a standard normal variable. Then, all subsequent realizations are conditional upon all previous simulations. Following Eq. (16), once simulated, Z_n becomes a data point in the vector $\boldsymbol{Z}_p$ to be conditioned upon by all subsequent data locations. This process is repeated by following a random path to each unknown location until all the values in the field have been simulated.

It should be noted that the spatial dependence and the conditional simulation algorithm introduced above are for variables having a Gaussian distribution. For non-Gaussian distributions, the inference of spatial structure is recommended to be performed on transformed data using a normal score mapping (Goovaerts, 1997). Such normal score mapping is a common practice in many applications of geostatistics and has previously been shown to preserve the prescribed spatial structure for lognormally distributed variables in various applications (Chen et al., 2012; Baker et al., 2011; Wang et al., 2017; Wang and Chen, 2017).

The above described random field models are implemented in Matlab and will be coupled with the multiphysics finite element model described in Section 4 to simulate dynamic responses of the heterogeneous seabed with an embedded pipeline. Fig. 3 is a schematic illustration of the multiresolution random field, where higher resolution random field is generated around the embedded pipeline.

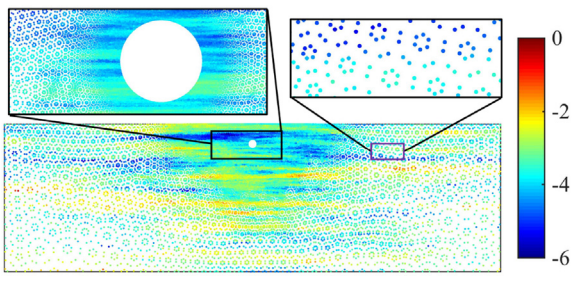

Fig. 3. A schematic illustration of the multiresolution random filed. The property shown is the seabed hydraulic conductivity in log10 scale.

3.3. Statistical and spatial characteristics of seabed properties

In the context of the hydromechanical coupled problem formulated in Section 2, seabed properties of interest include hydraulic conductivity, porosity, density, elastic properties (e.g., shear modulus, Young's modulus). Among them, hydraulic conductivity, porosity, and shear modulus are often considered as the primary parameters influencing the hydromechanical responses of the seabed (Zhang et al., 2016; Jeng, 2012). Hydraulic conductivity and porosity can be considered dependent on each other, e.g., through the Kozeny-Carman relationship and the fact that hydraulic conductivity can be related to the intrinsic permeability of the porous media. Hence, in this study, only hydraulic conductivity and shear modulus will be treated as spatially correlated random variables. Impact of the heterogeneous hydraulic conductivity and shear modulus fields will be analyzed through multiphysics finite element simulations.

Statistical and spatial characterizations of seabed properties are difficult to obtain due to very limited field data of marine soil. Table 1 summarizes some examples of seabed properties from previous research on marine soils.

In this work, statistical and spatial characteristics of the random field variables, in particular, the coefficient of variation (COV) and the correlation length parameters (θ_x, θ_z), are chosen based on prior researches and parametric studies will also be conducted to evaluate the influence of statistical and spatial parameters. Both the shear modulus and hydraulic conductivity are assumed to follow lognormal distributions in this work. While there lacks clear evidence pointing to a specific probability distribution of seabed properties, one condition that

Table 1
Statistical and spatial characteristics of marine soils from previous research.

Parameter	Statistical and spatial characteristics	Location and Reference
Hydraulic conductivity K	Mean: $0.3 \sim 6.1 \times 10^{-4}$ m/s	Fort Walton Beach, Florida (Bennett et al., 2002; Schock, 2004)
	Mean: 2.3×10^{-6} m/s	East sea, China (Wu et al., 2015)
	Mean: $10 \sim -510^{-8}$ m/s	Saga, Japan (Shen et al., 2015)
	Mean: 8.9×10^{-4} m/s	Sau Mau Ping, Hong Kong (Zhang et al., 2004, 2016)
	COV: 60% ~ 200%	Sau Mau Ping, Hong Kong (Zhang et al., 2004, 2016)
	Vertical correlation: 0.8 ~ 1.6 m	Columbus, Mississippi (Rehfeldt et al., 1992)
	Horizontal correlation: 4.8 ~ 12.8 m	Columbus, Mississippi (Rehfeldt et al., 1992)
Shear modulus G_s	Mean: 1.0 ~ 6.0 MPa	Mississippi River Delta (Yamamoto and Torii, 1986)
	Mean: 22 ~ 31 MPa	Genova Harbour (Grasso et al., 2012)
	Mean: 15.5 ~ 207 MPa	Key Biscayne, Florida (Trevorrow and Yamamoto, 1991)
	COV: 15% ~ 95%	Recommendation by (Phoon and Kulhawy, 1999a)
	Vertical correlation: 0.5 ~ 3.0 m	Recommendation by (Jiang et al., 2014)
	Horizontal correlation: 10 ~ 40 m	Recommendation by (Jiang et al., 2014)

has to be satisfied is for the probability density function to have a non-negative lower bound. To this end, the lognormal distribution is widely used to describe soil properties. Experimental data for shear modulus and hydraulic conductivity are usually found to follow a lognormal distribution (e.g. (Phoon and Kulhawy, 1999b; Baecher and Christian, 2005; Carsel and Parrish, 1988),). The lognormal distribution was also used for seabed properties in a recent study (Zhang et al., 2016). Anisotropy of the random field will be realized by skewing the ratio of the scalar parameter θ_x and θ_z in Eq. (11).

4. Multiphysics finite element model

In this section, details of the multiphysics finite element implementation are presented. The finite element model will be coupled with the multiresolution random field model described in Section 3 to simulate the dynamic response of a heterogeneous seabed-pipeline system.

4.1. Numerical implementation

The COMSOL Multiphysics software is used to implement the hydromechanical problem formulated in Section 2 and to simulate dynamic responses of a heterogeneous seabed-pipeline system. One advantage of using COMSOL in this study is that, through its *LiveLink for Matlab* interface, the COMSOL solver can be integrated with the random field code implemented in Matlab. This convenient interface between multiphysics finite element solver and random field code allows running many instances of Monte Carlo simulations needed to study the impact of heterogeneous seabed on the system responses.

The governing equations, i.e., PDEs, are implemented in COMSOL through its *General Form PDE* mode. Substituting the constitutive laws Eqs. (5) and (6) for porous seabed and solid pipeline into their corresponding balance laws Eqs. (1), (3) and (4), and using small strain displacement relations, the implemented governing equations for the porous seabed are written as

$$K_x\frac{\partial^2 p}{\partial^2 x} + K_z\frac{\partial^2 p}{\partial^2 z} - \phi_f\rho_f g\beta\frac{\partial p}{\partial t} = -\rho_f\frac{\partial^2}{\partial^2 t}\left(K_x\frac{\partial u}{\partial x} + K_z\frac{\partial w}{\partial z}\right) + \rho_f g\frac{\partial}{\partial t}\left(\frac{\partial u}{\partial x} + \frac{\partial w}{\partial z}\right) \tag{17}$$

$$\frac{\partial p}{\partial x} = -\rho\frac{\partial^2 u}{\partial^2 t} + G_s\left(\frac{\partial^2 u}{\partial^2 x} + \frac{\partial^2 u}{\partial^2 z}\right) + \frac{1}{1-2\nu_s}G_s\frac{\partial}{\partial x}\left(\frac{\partial u}{\partial x} + \frac{\partial w}{\partial z}\right) + \rho b_x \tag{18}$$

$$\frac{\partial p}{\partial z} = -\rho\frac{\partial^2 w}{\partial^2 t} + G_s\left(\frac{\partial^2 w}{\partial^2 x} + \frac{\partial^2 w}{\partial^2 z}\right) + \frac{1}{1-2\nu_s}G_s\frac{\partial}{\partial z}\left(\frac{\partial u}{\partial x} + \frac{\partial w}{\partial z}\right) + \rho b_z \tag{19}$$

where u and w are the horizontal (x) and vertical (z) component of the displacement vector; p is the excess pore pressure; K_x and K_z are the x and z components of the hydraulic conductivity tensor; G_s is the shear modulus of the seabed; ν_s is the Poisson's ratio; ϕ_f is the volume fraction of the void; ρ_f is the intrinsic mass density of the fluid; ρ is the equivalent density of the porous seabed; g is the gravitational acceleration; β is given in Eq. (2); b_x and b_z are the x and z components of the body force.

Similarly, the governing equations for the pipeline can be derived and are written as

$$-\rho_p\frac{\partial^2 u}{\partial^2 t} + G_p\left(\frac{\partial^2 u}{\partial^2 x} + \frac{\partial^2 u}{\partial^2 z}\right) + \frac{1}{1-2\nu_p}G_p\frac{\partial}{\partial x}\left(\frac{\partial u}{\partial x} + \frac{\partial w}{\partial z}\right) + \rho_p b_x = 0 \tag{20}$$

$$-\rho_p\frac{\partial^2 w}{\partial^2 t} + G_p\left(\frac{\partial^2 w}{\partial^2 x} + \frac{\partial^2 w}{\partial^2 z}\right) + \frac{1}{1-2\nu_p}G_p\frac{\partial}{\partial z}\left(\frac{\partial u}{\partial x} + \frac{\partial w}{\partial z}\right) + \rho_p b_z = 0 \tag{21}$$

where G_p is the shear modulus of the pipeline; ν_p is the Poisson's ratio; ρ_p is the density of the pipeline.

In addition to governing equations, the dynamic wave pressure equation Eq. (8) is also implemented in COMSOL as a user-defined boundary condition. Once the governing equations and boundary conditions are implemented, solutions u, w and p will be obtained through the COMSOL multiphysics solver.

4.2. Model validation - pipeline in a homogeneous seabed

Before coupling the implemented COMSOL multiphysics model with the multiresolution random field model, the multiphysics model is first validated using experimental data reported in (Turcotte et al., 1984). The experiments have a similar setup to the schematic diagram shown in Fig. 1. The seabed is simulated using a sediment bay with a PVC pipe inside it simulating the buried pipeline. The seabed-pipeline system is then placed in a large wave tank, which can stimulate waves of specific characteristics. Most of the material properties of the seabed have been previously calibrated and reported in (Cheng and Liu, 1986) except water characteristics and mass density of seabed, which are reported in (Zhou et al., 2013). The properties of the PVC pipe from (Rajani et al., 1996) are used in the validation. Model geometry, wave, seabed and pipeline characteristic are all summarized in Table 2.

Numerical solutions of the normalized excess pore pressure around the pipeline are obtained using the multiphysics model and then compared against the data measured in physical experiments from (Turcotte et al., 1984). The comparisons are plotted in Fig. 4. It can be seen that results from numerical simulations and physical experiments are in reasonable agreements. The numerical model is able to correctly capture the response of the seabed-pipeline system.

Table 2
Model parameters and material properties for validation test; [a] and [b] indicate two test cases, each with different wave characteristics as reported in (Turcotte et al., 1984).

Wave characteristics			
Wave height (H)	0.0524[a], 0.143[b] (m)	Water depth (d)	0.533 (m)
Wave period (T)	0.9[a], 1.75[b] (s)	Wavelength (L)	1.25[a], 3.54[b] (m)
Water characteristics			
Mass density (ρ_f)	1000 (kg/m^3)	Bulk modulus (k_f)	2×10^3 (MPa)
Seabed characteristics			
Seabed thickness (h)	0.826 (m)	Mass density (ρ)	1400 (kg/m^3)
Seabed length (l)	4.57 (m)	Shear modulus (G_s)	0.64 (MPa)
Poisson's ratio (ν_s)	0.33	Hydraulic conductivity (K)	0.0011 (m/s)
Porosity (n)	0.42	Degree of saturation (S_r)	0.95
Pipeline characteristics			
Shear modulus (G_p)	790 (MPa)	Mass density(ρ_p)	1450 (kg/m^3)
Thickness (t_p)	0.02 (m)	Outer diameter (D_p)	0.168 (m)
Poisson's ratio (ν_p)	0.42	Buried depth (e)	0.167 (m)

Table 3
Boundary conditions of the example problem. The wave pressure $p_b(t)$ is the wave-induced loading defined by Eq. (8). Note that the degrees of freedom of the porous seabed are denoted as u_s, w_s and p, and degrees of freedom of the pipeline are denoted as u_p and w_p.

Boundary	Fluid flow	Elasticity
Top $z = 0$	Wave pressure $p_b(t)$	free: $\sigma_{zz} = 0$, $\sigma_{xz} = 0$
lateral $x = \pm 50$	no flux $q = 0$	roller $u_s = 0$
pipe and seabed interface	impermeable	$u_s = u_p$, $v_s = v_p$
bottom $z = -30$	no flux $q = 0$	fixed $u_s = v_s = 0$

4.3. Model setup - pipeline in a heterogeneous seabed

In this section, the multiphysics model is coupled with the multi-resolution random field model to simulate the response of a pipeline embedded in a heterogeneous seabed. The model domain (Fig. 5) is 100 m wide and 30 m deep. A pipeline, 2.0 m in diameter and 0.2 m in thickness, is horizontally centered in the seabed and buried 4.0 m below the seabed surface. A wave with 6.0 m in height (H) and 70.93 m in length (L) is generated following Eq. (8). The seabed domain is set to be slightly wider than one full wavelength so that a full wave-induced loading can be modeled. The depth of the seabed (30 m) is about five times the wave height, where the wave-induced effects on the seabed become negligible.

Boundary conditions of the model problem are summarized in Table 3.

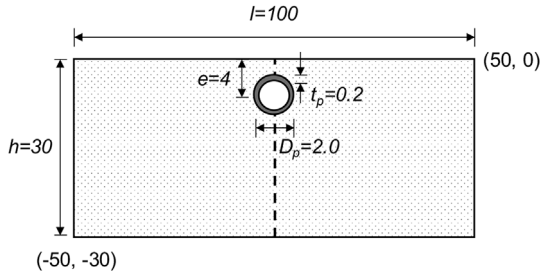

Fig. 5. The sketch of the model geometry (unit: m). The boundary conditions are given in Table 3.

Table 4
Input parameters for the hydromechanical coupled problem. ⋆ indicates the mean value.

Wave characteristics			
Wave height (H)	6 (m)	Water depth (d)	5 (m)
Wave period (T)	8 (s)	Wavelength (L)	70.93 (m)
Water characteristics			
Mass density (ρ_f)	1000 (kg/m^3)	Bulk modulus (k_f)	2×10^3 (MPa)
Seabed characteristics			
Seabed thickness (h)	30 (m)	Mass density (ρ)	1400 (kg/m^3)
Seabed length (l)	100 (m)	Shear modulus⋆ (G_s)	10 (MPa)
Poisson's ratio (ν_s)	0.4	Hydraulic conductivity⋆ (K)	5.0×10^{-4} (m/s)
Porosity (n)	0.4	Degree of saturation (S_r)	0.99
Pipeline characteristics			
Shear modulus (G_p)	6.8×10^4 (MPa)	Mass density (ρ_p)	2700 (kg/m^3)
Thickness (t_p)	0.2 (m)	Outer diameter (D_p)	2.0 (m)
Poisson's ratio (ν_p)	0.32	Buried depth (e)	4.0 (m)

The input model parameters and material properties are summarized in Table 4. Those parameters are chosen based on prior knowledge from literature (Table 1) and the author's previous experience (Zhou et al., 2013, 2014). In (Jeng and Cheng, 1999), pipeline diameters ranging from 1 to 3 m and burial depths ranging from 1.5 to 4 m were investigated in the case study. The geometry and burial depth are known to significantly influence the distribution of the pore pressure (Jeng and Lin, 1999; Jeng and Cheng, 1999). The choice of pipeline geometry and burial depth will depend on specific applications. The water depth and wave characteristic values are taken from a previous study (Zhou et al., 2013) and correspond to the case of waves in shallow water. For the hydraulic conductivity K and shear modulus G_s of the porous seabed, as discussed in Section 3, they are treated as spatially correlated random variables and modeled through multiresolution

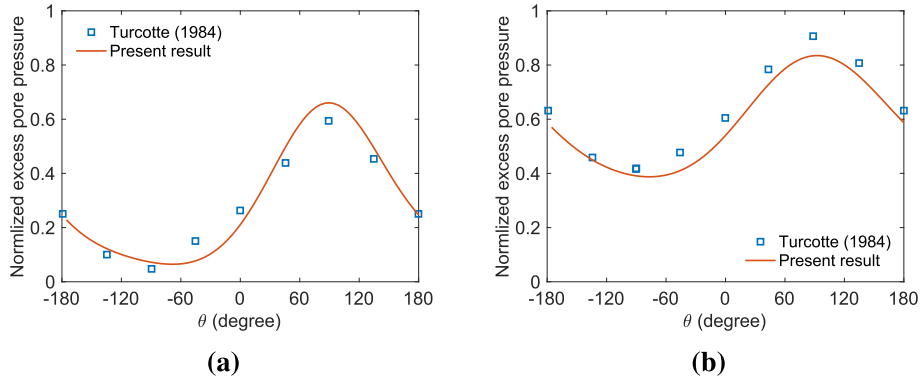

Fig. 4. Validation of the multiphysics model with the experimental data available from (Turcotte et al., 1984). The excess pore pressure is normalized by the amplitude of the wave pressure at the seabed surface p_0 and θ is the angle of the measurement point counterclockwise from the horizontal direction.

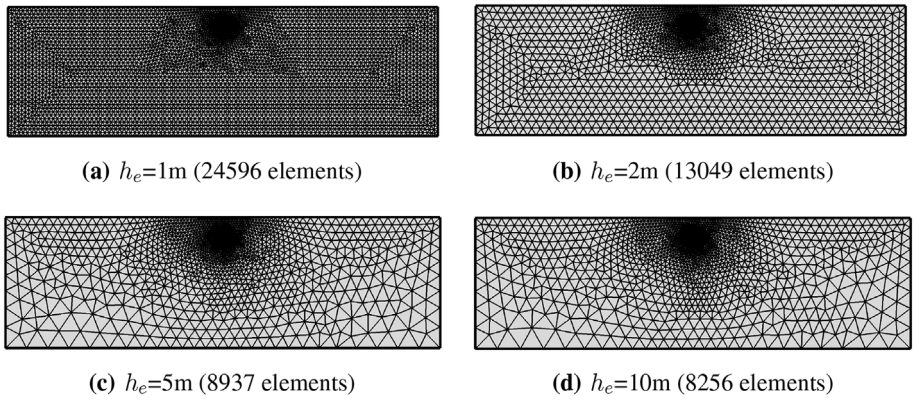

(a) h_e=1m (24596 elements) **(b)** h_e=2m (13049 elements)

(c) h_e=5m (8937 elements) **(d)** h_e=10m (8256 elements)

Fig. 6. The four meshes used in the mesh sensitivity analysis. h_e indicates the maximum element size in the problem domain.

random field models.

4.4. Mesh sensitivity analysis

The implemented multiphysics finite element will be coupled with random field models to study responses and associated uncertainties of a heterogeneous seabed-pipeline system using Monte Carlo simulations. This requires a large number of simulations. An extremely fine finite element, though more accurate, may be computationally too expensive for such purpose. To this end, a mesh sensitivity analysis is first carried out to obtain an optimal mesh to be used for the following Monte Carlo simulations.

To ensure sufficient resolution and accuracy of solutions around the embedded pipeline, a relatively fine discretization is used by enforcing 80 nodes around the pipeline circumference. The mesh sensitivity analysis is carried out by changing the maximum element size h_e in the domain. As h_e increases, the total number of elements in the domain decreases. Note that when the maximum element size h_e is sufficiently large, the total number of elements will not change as much due to the fact that an extremely fine resolution is enforced around the pipeline. Fig. 6 shows four different finite element meshes and Table 5 summarizes the total number of elements and runtime for each mesh.

The performance of different meshes is evaluated by extracting and comparing quantities of interest, in particular, the excess pore pressure in the seabed, the von Mises stress in the pipeline, the vertical displacement at the top of the pipeline and the area ratio of transient liquefaction. Fig. 7 summarizes the mesh sensitivity study results. Based on the mesh sensitivity results and considering the trade-off between runtime and accuracy, the mesh with $h_e = 5$ is selected for the following Monte Carlo simulations and the results will be presented and discussed in Section 5.

4.5. Convergence of Monte Carlo simulations

To study the impact of material heterogeneities and associated uncertainties on the seabed-pipeline system, a sufficient number of Monte Carlo simulations is needed. Fig. 8 shows the variations of mean and coefficient of variation (COV) of displacement at the top of the pipeline and the maximum von Mises stress in the pipeline with the number of Monte Carlo simulations. It can be observed that 1000 Monte Carlo simulations are sufficient for the given example problem and will be used in the numerical analysis and discussions.

Table 5
Summary of mesh sensitivity analysis. * Simulations are performed on a workstation using a single core of an Intel Xeon(R) CPU E3-1241 v3 @ 3.5 GHz with 8 Gb RAM.

h_e (m)	Number of elements	runtime* (s)
1	24596	170.08
2	13049	75.06
5	8937	72.52
10	8256	69.66

5. Numerical results and discussions

In this section, numerical results of the coupled multiresolution random field and multiphysics finite element simulations are presented. Effects of heterogeneous seabed properties and wave-induced loading on the dynamic responses of the system will be analyzed in details. The hydraulic conductivity and shear modulus of the seabed are treated as spatially correlated but statistically independent random variables. Three parameters, i.e., the coefficient of variance (COV), the horizontal and vertical correlation length parameters (θ_x, θ_z) are the three main random field parameters controlling the heterogeneous attributes of the seabed. Parametric studies of these parameters will also be conducted to understand and quantify their influence on system responses. Other input parameters for the model have been summarized in Table 4.

5.1. Effects of spatially correlated hydraulic conductivity fields

For the heterogeneous spatially correlated hydraulic conductivity fields, the three main random parameters are set at COV = 2.5, $\theta_x = 20$ m and $\theta_z = 1$ m considering ranges summarized in Table 1. The mean of the hydraulic conductivity field is 5×10^{-4} m/s and a log-normal distribution is assumed. 1000 Monte Carlo simulations are performed to assess the effects and the associated uncertainties.

A typical realization of the heterogeneous hydraulic conductivity field and the corresponding hydromechanical responses (i.e., displacements and excess pore pressure distribution) at a particular time (t = 4 s) are shown in Fig. 9. The random field realization clearly shows layered profiles in the horizontal direction, consistent with the high ratio of θ_x/θ_z. The excess pore pressure peaks near the surface and decreases with depth as expected. Displacement profiles show that there is not much horizontal displacement around the pipeline but the vertical displacement is relatively large.

As for the response of the pipeline, a particular quantity of interest is the stress in the pipeline. Fig. 10 shows the von Mises stress in the pipeline at time t = 2, 4 s corresponding to the heterogeneous hydraulic conductivity field shown in Fig. 9(a). It can be seen that the maximum von Mises stress is located around the inner surface of the pipeline and the distribution is not symmetric due to the heterogeneous nature of the surrounding seabed.

To quantify the effects and associated uncertainties of the heterogeneous hydraulic conductivity fields on the hydromechanical responses of the seabed-pipeline system, characteristic responses of the system are extracted and calculated based on 1000 Monte Carlo simulations. These responses include the maximum von Mises stress in the

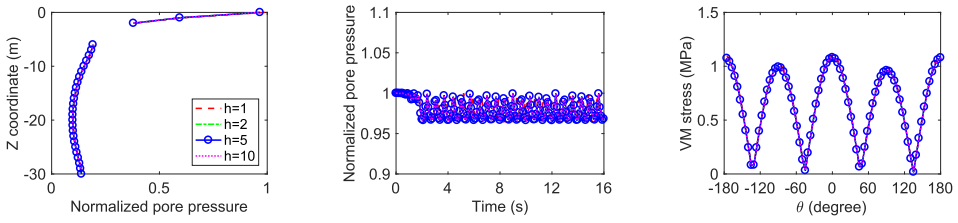

(a) Pore pressure at cut line x=0, t=8s **(b)** Maximum normalized excess pore pressure **(c)** von Mises stress along inside circumference

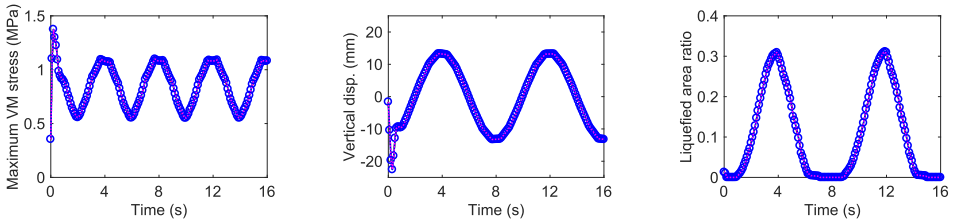

(d) Maximum von Mises stress in pipeline **(e)** Vertical displacement at x=0, z=-3 m **(f)** Area ratio of liquefaction

Fig. 7. Comparison of simulation results obtained with different meshes. The excess pore pressure is normalized by the amplitude of the wave pressure at the seabed surface p_0. VM in the y-axis stands for von Mises. Note that these figures share the same legend.

pipeline, the vertical displacement at the top of the pipeline, the excess pore pressure along a vertical line cut through the center of the pipeline and the area ratio of liquefaction defined by Eq. (9). For comparison, results of a homogeneous field with a hydraulic conductivity value equal to the mean of the heterogeneous field are also included. The results are plotted and grouped in Fig. 11. It is interesting to see that, even with a very large COV in the hydraulic conductivity field, the quantities evaluated from heterogeneous model do not deviate as much from the corresponding homogeneous model. For instance, the vertical displacement curves shown in Fig. 11(b) almost coincide with each other. The influences of the heterogeneous hydraulic conductivity fields on the maximum von Mises stress in the pipeline and the area ratio of liquefaction are more noticeable but still relatively insignificant. Similar observations have been made in a previous study (Zhang et al., 2016) that the spatially varying hydraulic conductivity fields do not significantly affect the hydromechanical response of the seabed, though no embedded pipeline was included in the previous study.

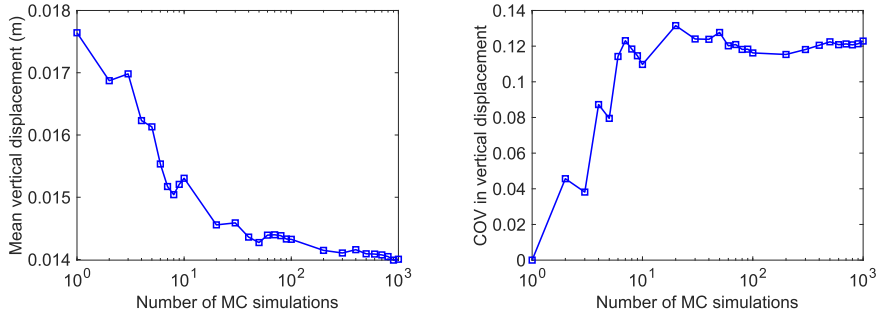

(a) Mean vertical displacement **(b)** COV vertical displacement

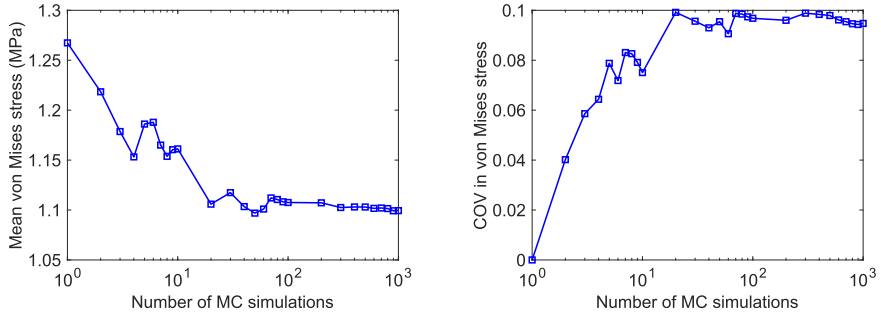

(c) Mean von Mises **(d)** COV von Mises

Fig. 8. Convergence of Monte Carlo simulations to the statistics of system responses of interest.

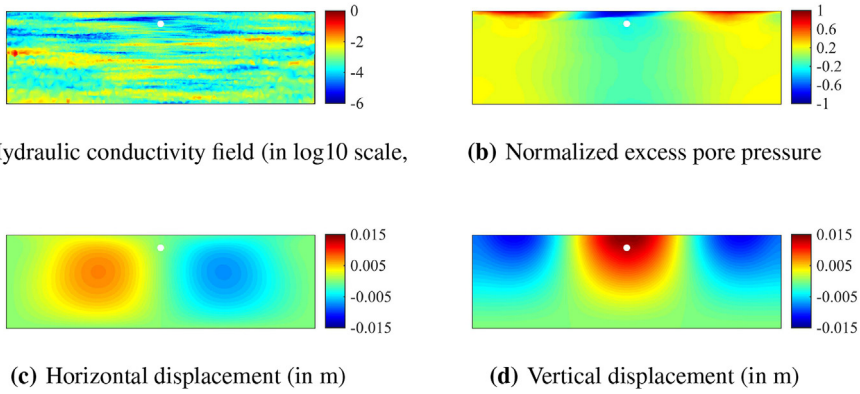

(a) Hydraulic conductivity field (in log10 scale, m/s)

(b) Normalized excess pore pressure

(c) Horizontal displacement (in m)

(d) Vertical displacement (in m)

Fig. 9. A typical random field realization of the hydraulic conductivity field and the corresponding hydromechanical responses at time $t = 4$ s. The hydraulic conductivity field is plotted in log10 scale and the excess pore pressure is normalized by the amplitude of the wave pressure at seabed surface p_0.

5.2. Sensitivity analysis of hydraulic conductivity

To gain more insights into the effects of hydraulic conductivity on the hydromechanical response of the seabed-pipeline system, a sensitivity analysis is conducted. The sensitivity analysis is carried out using homogeneous models, each with a constant hydraulic conductivity field. A wider range of hydraulic conductivity values, ranging from 5×10^{-6} m/s to 5×10^{-2} m/s, is considered.

The characteristic responses, in terms of the maximum von Mises stress in the pipeline, the maximum vertical displacement in the seabed and the area ratio of liquefaction, are summarized in Fig. 12. All these responses exhibit no noticeable variations at low hydraulic conductivity, from 5×10^{-6} to 5×10^{-4} m/s. In particular, the maximum von Mises stress in the pipeline and the maximum vertical displacement at the top of the pipeline are insensitive to varying hydraulic conductivity values. For hydraulic conductivity higher than 5×10^{-4} m/s, the area ratio of liquefaction reduces significantly with the increasing hydraulic conductivity, due to the fact that a higher hydraulic conductivity increases the dissipation rate of excess pore pressure. When heterogeneous hydraulic conductivity fields are introduced, a certain area in the seabed would possess high hydraulic conductivity, which would affect the pore pressure and furthermore the area ratio of liquefaction in that local area. However, the global effects of the heterogeneous hydraulic conductivity fields would be relatively small due to space averaging effect. It is consistent with the aforementioned discussion that the influences of the heterogeneous hydraulic conductivity fields on the area ratio of liquefaction is more noticeable, but still relatively insignificant. Overall, in the example problem where an average value 5×10^{-4} m/s of the hydraulic conductivity is considered, its spatial variability effects on hydromechanical response are relatively insignificant.

5.3. Effects of spatially correlated shear modulus fields

For the heterogeneous spatially correlated shear modulus field, the following parameters are used considering ranges of those parameters summarized in Table 1: the three main random parameters are set at COV = 0.3, $\theta_x = 20$ m and $\theta_z = 1$ m. Parametric studies on these parameters will be presented in a subsequent section. The mean of the shear modulus is 10 MPa and a lognormal distribution is assumed. As in the case of the heterogeneous hydraulic conductivity fields, a total of 1000 Monte Carlo simulations are performed to assess the impacts of the heterogeneous shear modulus fields and the associated uncertainties.

A typical realization of the heterogeneous shear modulus field and the corresponding hydromechanical responses (i.e., displacements and excess pore pressure distribution) at a particular time (t = 4 s) are shown in Fig. 13. As in the previous hydraulic conductivity case, the random field shows layered profiles due to the specified anisotropy by skewing the ratio of θ_x and θ_z in Eq. (11).

Fig. 14 shows the von Mises stress in the pipeline at time t = 2, 4 s corresponding to the heterogeneous shear modulus field. The inner surface of the pipeline is predicted to experience the maximum von Mises stress. The locations of the maximum von Mises stress are further away from the vertical and horizontal symmetric lines due to the influence of surrounding heterogeneous soils.

Based on the results of 1000 Monte Carlo simulations, characteristic responses of the system are shown in Fig. 15. It can be seen that, even with a smaller COV (0.3 in the shear modulus compared to 2.5 in the hydraulic conductivity case), responses of the system are greatly

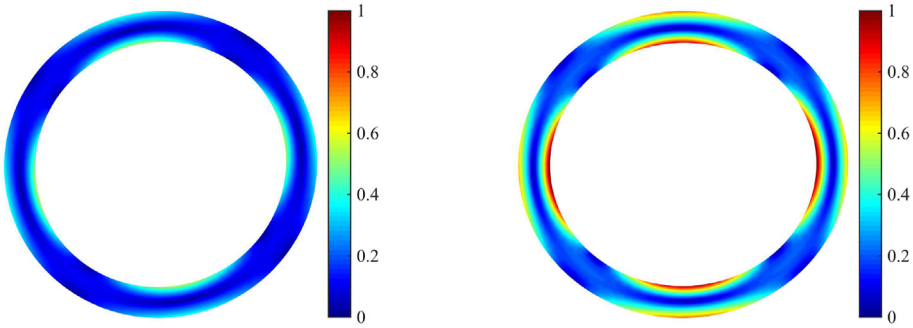

(a) t = 2 s

(b) t = 4 s

Fig. 10. Distribution of von Mises stress (in MPa) in the pipeline for seabed with heterogeneous hydraulic conductivities. Solid grey lines indicate the original shape of the pipeline. The deformation is scaled by a factor of 1000.

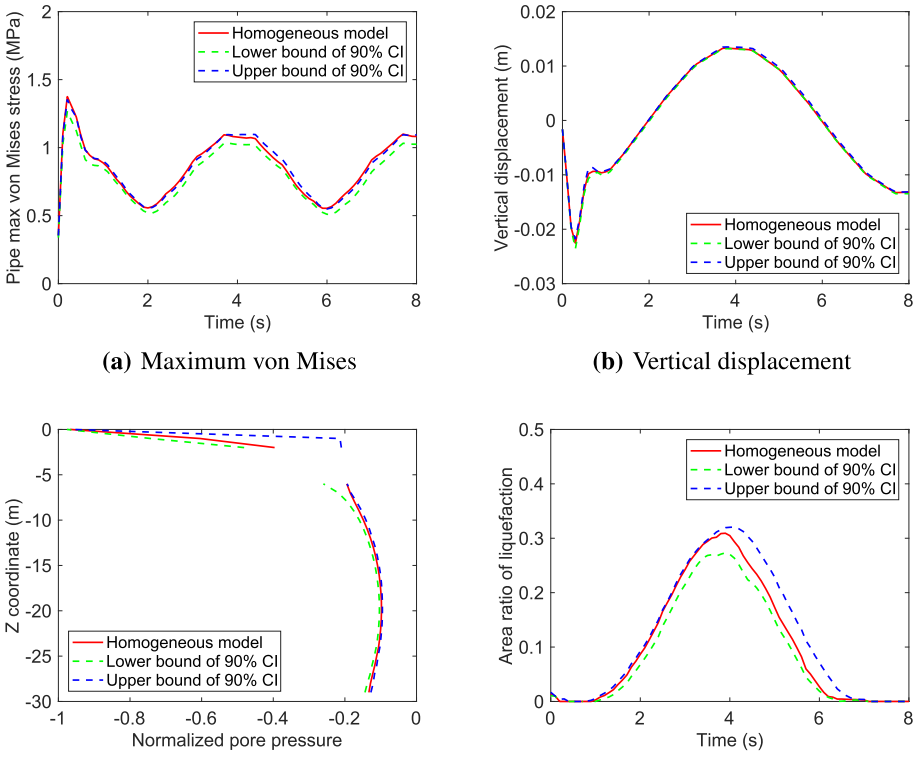

(a) Maximum von Mises **(b)** Vertical displacement

(c) Excess pore pressure **(d)** Area ratio of liquefaction

Fig. 11. Characteristic responses of the seabed-pipeline system with heterogeneous hydraulic conductivity field. The associated uncertainties are expressed in terms of 90% confident intervals (CI). (a) the maximum von Mises stress in the pipeline; (b) the vertical displacement at the top of the pipeline; (c) the excess pore pressure along a vertical line cut through the pipeline; and (d) the area ratio of liquefaction around the pipeline.

affected. For instance, Fig. 15(c) shows that, even at a deep depth ($z = 30$ m), the excess pore pressure generated by the heterogeneous fields is almost twice of the homogeneous counterpart. As for the von Mises stresses and vertical displacement, impacts of heterogeneous shear modulus fields are also more significant compared to the hydraulic conductivity fields.

5.4. Parametric study of the shear modulus coefficient of variation

In the first parametric study, the random parameter COV of the shear modulus field is set with the following values: 0.15, 0.3, 0.45, 0.6, 0.75, and the other two random parameters $\theta_x = 20$ m, $\theta_z = 1$ m are kept constant. The mean of the shear modulus field is 10 MPa. For each set of random parameters, 1000 Monte Carlo simulations are performed, resulting in a total of 5000 Monte Carlo simulations.

Fig. 16 shows the statistics of the characteristic hydromechanical responses, including the maximum von Mises stress in the pipeline, the vertical displacement at the top of the pipeline, and the area ratio of liquefaction around the pipeline. The uncertainties of these characteristic responses, quantified in terms of their COV, are all observed to be increasing with the increasing coefficient of variance of the shear moduli, as shown in Fig. 16(d), (e) and (f). It is consistent to common engineering perception that, if considering hydromechanical responses as model outputs and the shear moduli property as model inputs, the uncertainty of the model outputs would be positively correlated to the uncertainty of the model inputs. A similar phenomenon was observed in (Griffiths and Fenton, 2001; Griffiths et al., 2002), where the uncertainty of the bearing capacity increases with the increasing uncertainty in input soil parameters. It is interesting to note that, within the examined range of COVs in the shear modulus field, the uncertainties of the characteristic responses of the system increase monotonously and almost linearly with the increasing uncertainty of the shear modulus field.

The relations between the mean of the characteristic responses and the COVs in shear modulus field are shown in Fig. 16(a), (b) and (c). It is observed that the mean von Mises stress and the mean vertical displacement are increasing with the increasing uncertainty of the shear moduli, but the area ratio of liquefaction around the pipeline actually decreases with the increasing uncertainty in the shear modulus field.

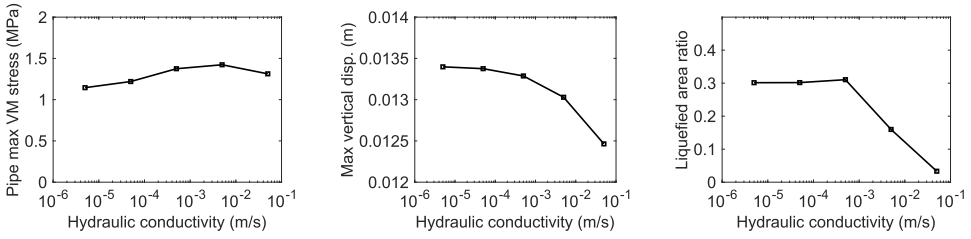

(a) Maximum von Mises stress **(b)** Maximum vertical displacement **(c)** Area ratio of liquefaction

Fig. 12. The sensitivity of the characteristic responses of the seabed-pipeline system to the hydraulic conductivity: (a) the maximum von Mises stress in the pipeline, (b) the maximum vertical displacement in the seabed, and (c) the area ratio of liquefaction around the pipeline.

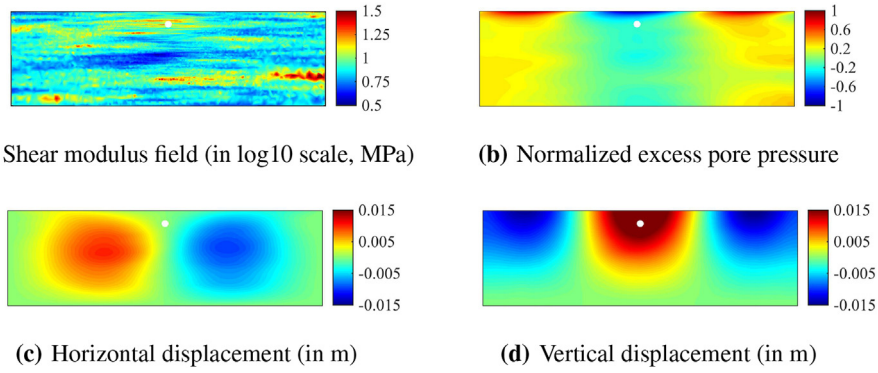

(a) Shear modulus field (in log10 scale, MPa) **(b)** Normalized excess pore pressure

(c) Horizontal displacement (in m) **(d)** Vertical displacement (in m)

Fig. 13. A typical random field realization of the shear modulus field and the corresponding hydromechanical responses at time $t = 4$ s. The hydraulic conductivity field is plotted in log10 scale and excess pore pressure is normalized by the amplitude of the wave pressure at the seabed surface p_0.

5.5. Parametric study of the shear modulus spatial correlations

In the second parametric study, the shear modulus horizontal spatial correlation length θ_x is set with the following values: 2, 4, 10, 20, 40, 100 m. The vertical spatial correlation length is varied accordingly by keeping a constant ratio of $\theta_x/\theta_z = 20$. The COV of the shear modulus field is kept constant at 0.3. The mean of the shear modulus field is 10 MPa. Example realizations of shear modulus fields with different horizontal spatial correlation lengths are shown in Fig. 17. As expected, when the spatial correlation length approaches zero, the soil property tends to be spatially independent, i.e. the soil property at any position is a random variable itself and will not be affected by the value of its neighboring position. As the correlation length approaches a very large value (compared to the domain size), the seabed becomes more of a multi-layered field, where the seabed properties vary as random variables within each layer.

Again, 1000 Monte Carlo simulations are performed for each set of random field parameters. Characteristic hydromechanical responses of the seabed-pipeline system, i.e., the maximum von Mises stress in the pipeline, the vertical displacement at the top of the pipeline, and the area ratio of liquefaction, are evaluated and examined. The statistics of these responses are summarized in Fig. 18. It can be seen that there are no significant changes in the mean of these responses within the considered wide range of the horizontal spatial correlation length, as shown in Fig. 18(a), (b), and Fig. 18(c). This indicates that, for the given example problem, the spatial correlation length has a negligible influence on the mean values of the hydromechanical response. The uncertainties of these responses are observed to increase and then reach a plateau with the increasing spatial correlation length, as can be observed in Fig. 18(d), (e), and Fig. 18(f). As discussed at the beginning of this subsection, a spatially independent field of the shear moduli would evolve as the spatial correlation length approaches zero. Due to space averaging effect, the characteristic responses of such heterogeneous model would eventually approximate to that of a homogeneous model.

5.6. Implications of the inherent seabed heterogeneities on engineering design

Findings from the above analysis using the proposed framework have significant implications for the engineering design of submarine pipelines. The dynamic responses of the seabed-pipeline system are probabilistic in nature due to the inherent heterogeneities. The traditional design based on a homogeneous model of seabed could lead to unsafe designs. The obtained statistics of the characteristic hydromechanical responses can be utilized to inform and improve engineering design. To illustrate this point, the probability of insufficient design will be calculated based on Monte Carlo simulations. Here, an insufficient design is defined as a design case when the maximum von Mises stress in the pipeline evaluated from a heterogeneous model is higher than its value evaluated from a corresponding homogeneous model multiplied by a factor of safety. The probability of insufficient design is calculated as

$$P_f = P(\sigma_v^{het} > (\sigma_v^{hom} \cdot FS)) \tag{22}$$

where P_f denotes the probability of insufficient design; σ_v^{het} and σ_v^{hom} are the maximum von Mises stress in the pipeline evaluated from the heterogeneous model and the homogeneous model, respectively; FS is the factor of safety in design. This definition of insufficient design is motivated by the consideration that, if an engineer refers to the maximum von Mises stress evaluated from a homogeneous model as the basis pipeline design, there is a probability that such design is insufficient to carry the actual load even with a chosen factor of safety.

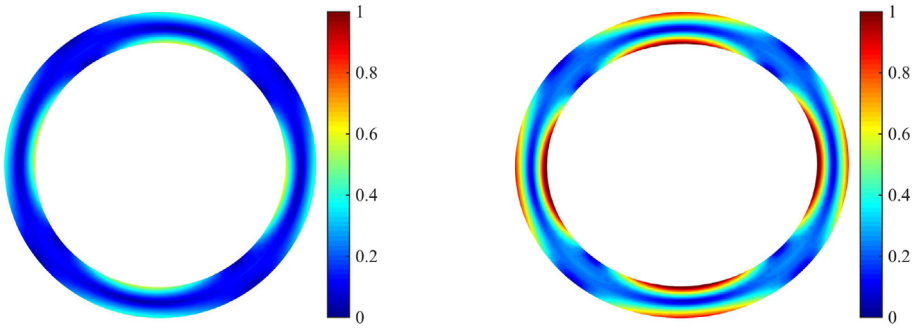

(a) t = 2 s **(b)** t = 4 s

Fig. 14. Distribution of von Mises stress (in MPa) in the pipeline for seabed with heterogeneous shear moduli. Solid grey lines indicate the original shape of the pipeline. The deformation is scaled by a factor of 1000.

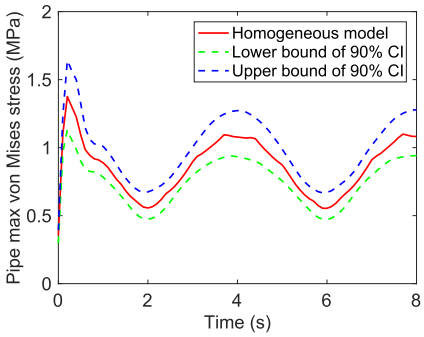

(a) Maximum von Mises stress

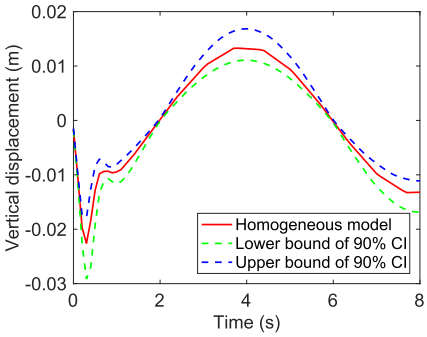

(b) Vertical displacement

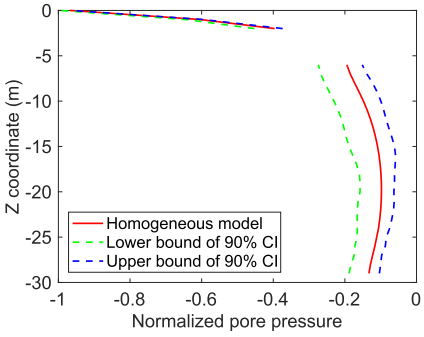

(c) Excess pore pressure

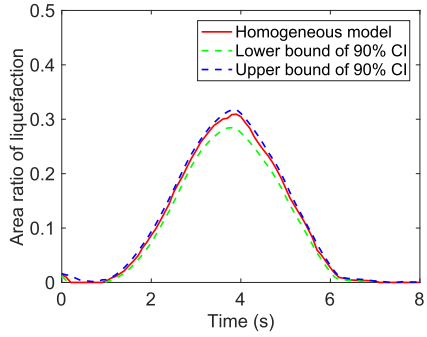

(d) Area ratio of liquefaction

Fig. 15. Characteristic responses of the seabed-pipeline system with heterogeneous shear modulus field. The associated uncertainties are expressed in terms of 90% confident intervals (CI). (a) the maximum von Mises stress in the pipeline; (b) the vertical displacement at the top of the pipeline; (c) the excess pore pressure along a vertical line cut through the pipeline; and (d) the area ratio of liquefaction around the pipeline.

Fig. 19 summarizes the probability of insufficient design with different factors of safety (FS) for a range of shear modulus COV and spatial correlation length values. Based on the definition in Eq. (22), the probability of insufficient design is a fixed number for a given set of Monte Carlo simulations (1000 in this study for each set of COV in shear modulus or spatial correlation length). This probability value may vary for a different number of Monte Carlo simulations. Since in this study the number of Monte Carlo simulations are set to 1000 based on the convergence results shown in Fig. 8, the COVs of the insufficient design probabilities do not need to be calculated.

Similar trends are observed in Fig. 19(a) for all $FS > 1.0$, i.e., the probability of insufficient design increases with the increasing COV. Take the case of $FS = 1.4$ as an example, the probability of insufficient design is close to zero for low COV of shear modulus field and it rises up to almost 12% if the COV increases to 0.75. The results indicate that a higher safety factor would be required if the seabed shear modulus is of high spatial variability. The relation between the probability of insufficient design and the spatial correlation length in Fig. 19(b) shows a similar trend. However, for the given factor of safety $FS = 1.4$, the probability of insufficient design remains relatively small within the wide ranges of spatial correlation length considered.

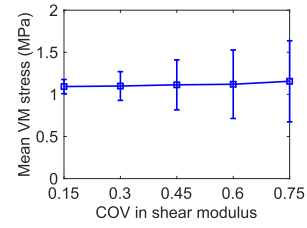

(a) Mean maximum von Mises stress

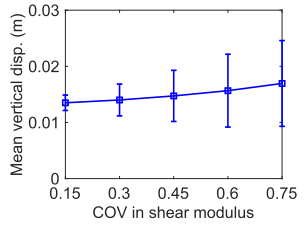

(b) Mean vertical displacement

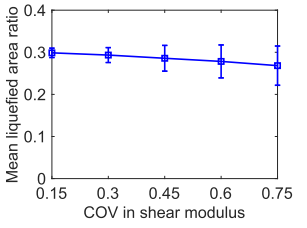

(c) Mean area ratio of liquefaction

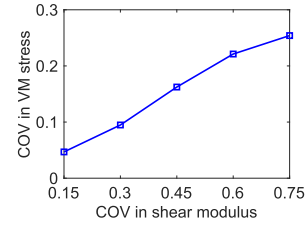

(d) COV of maximum von Mises stress

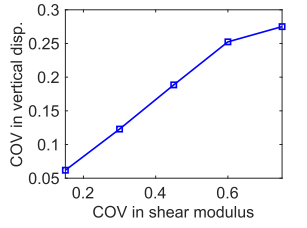

(e) COV of vertical displacement

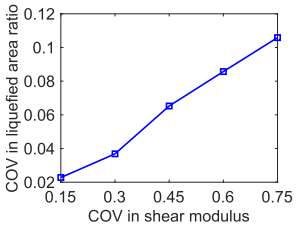

(f) COV of area ratio of liquefaction

Fig. 16. Statistics of the characteristic responses of the seabed-pipeline system as a function shear modulus COV at time t = 4 s: mean of (a) the maximum von Mises (VM) stress in pipeline, (b) the vertical displacement at the top of the pipeline, (c) the area ratio of liquefaction around the pipeline, and the COV of (d) the maximum von Mises stress in pipeline, (e) the vertical displacement at the top of the pipeline, (f) the area ratio of liquefaction around the pipeline.

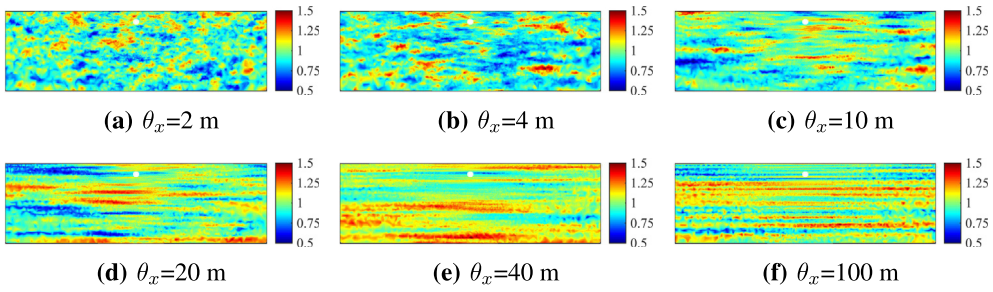

(a) θ_x=2 m (b) θ_x=4 m (c) θ_x=10 m

(d) θ_x=20 m (e) θ_x=40 m (f) θ_x=100 m

Fig. 17. Typical realizations of the heterogeneous shear moduli field (in log10 scale, unit in MPa) with different horizontal spatial correlation lengths θ_x.

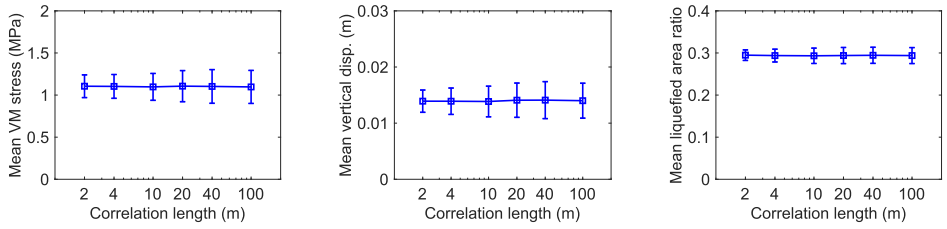

(a) Mean maximum von Mises stress (b) Mean vertical displacement (c) Mean area ratio of liquefaction

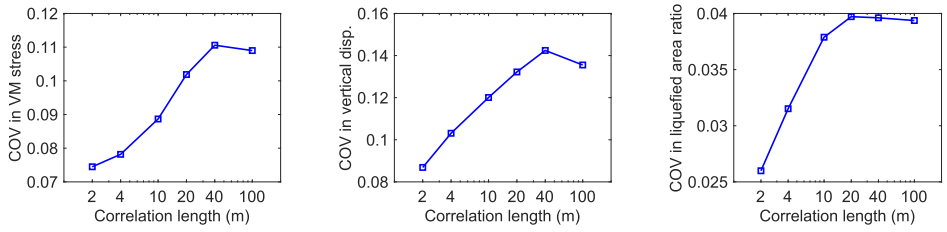

(d) COV of maximum von Mises stress (e) COV of vertical displacement (f) COV of area ratio of liquefaction

Fig. 18. Statistics of the characteristic responses of the seabed-pipeline system as a function of horizontal spatial correlation length at time t = 4 s: mean of (a) the maximum von Mises (VM) stress in pipeline, (b) the vertical displacement at the top of the pipeline, (c) the area ratio of liquefaction around the pipeline, and the COV of (d) the maximum von Mises stress in pipeline, (e) the vertical displacement at the top of the pipeline, (f) the area ratio of liquefaction around the pipeline.

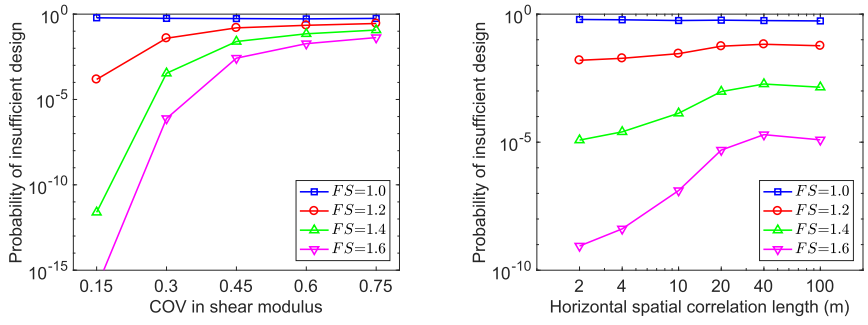

(a) Varying COV (b) Varying spatial correlation length

Fig. 19. Probabilities of insufficient design as function of the shear modulus field random parameter (a) COV and (b) horizontal spatial correlation length. Each point on the curve is evaluated using results from 1000 Monte Carlo simulations.

6. Conclusion

In this paper, the wave-induced dynamic responses of the seabed and embedded pipeline system are modeled, with the consideration of multiresolution heterogeneous seabed property fields and coupled hydromechanical simulations. The analysis model is first validated with experimental data of a pipeline embedded in homogeneous seabed sediment. The numerical model is able to correctly capture the response of the seabed-pipeline system. Then, the effects of heterogeneous hydraulic conductivity fields and heterogeneous shear moduli fields on the characteristic responses of the system are analyzed in details. Parametric studies on the effect of varying random parameters are also conducted. The statistics of the characteristic system responses are obtained from Monte Carlo simulations, which could be further utilized in informing engineering design. The main findings of this work are concluded as follows:

1. The characteristic responses of the pipeline, including the von Mises stress and displacement at the top are found to be insensitive to the spatially correlated hydraulic conductivity fields. The effects of hydraulic conductivity variability on the area ratio of liquefaction is more noticeable.
2. The spatial variability of seabed shear moduli has significant effects on the characteristic responses of the seabed-pipeline system. The

von Mises stress and displacement in the pipeline and the area ratio of liquefaction area around the pipeline can be significantly underestimated if a homogeneous model is used.
3. The uncertainty of the characteristic responses monotonously and almost linearly increases with the increasing COV of shear modulus field. And uncertainty of the characteristic responses firstly increases and then reaches to plateau with the increasing spatial correlation length of shear modulus field.
4. The statistics of the characteristic responses, obtained from Monte Carlo simulations, can be further utilized to inform probabilistic engineering design. For a given factor of safety, the probability of insufficient design increases with the increasing variability in the seabed properties.

Acknowledgment

This research is financially supported in part by the Shrikhande family foundation through the Shrikhande Graduate Fellowship and by the National Natural Science Foundation of China (Project No. 41572243 and 41372286). Clemson University is acknowledged for the generous allotment of computer time on the Palmetto high-performance computing facility.

References

Baecher, G.B., Christian, J.T., 2005. Reliability and Statistics in Geotechnical Engineering. John Wiley & Sons.
Baker, J.W., Seifried, A., Andrade, J.E., Chen, Q., 2011. Characterization of random fields at multiple scales: an efficient conditional simulation procedure and applications in geomechanics. Applications of Statistics and Probability in Civil Engineering 347.
Bennett, R.H., Hulbert, M.H., Curry, C., Johnson, H.P., Hutnak, M., Curry, K.J., 2002. In situ permeabilities of selected coastal marine sediments. IEEE J. Ocean. Eng. 27 (3), 571–580.
Carsel, R.F., Parrish, R.S., 1988. Developing joint probability distributions of soil water retention characteristics. Water Resour. Res. 24 (5), 755–769.
Chen, Q., Seifried, A., Andrade, J.E., Baker, J.W., 2012. Characterization of random fields and their impact on the mechanics of geosystems at multiple scales. Int. J. Numer. Anal. Methods GeoMech. 36 (2), 140–165.
Chen, Q., Wang, C., Juang, C.H., 2015. CPT-based evaluation of liquefaction potential accounting for soil spatial variability at multiple scales. J. Geotech. Geoenviron. Eng. 04015077. https://doi.org/10.1061/(ASCE)GT.1943-5606.0001402.
Cheng, A.H., Liu, P.L., 1986. Seepage force on a pipeline buried in a poroelastic seabed under wave loadings. Appl. Ocean Res. 8 (1), 22–32.
Gao, F., Jeng, D.S., Sekiguchi, H., 2003. Numerical study on the interaction between nonlinear wave, buried pipeline and non-homogenous porous seabed. Comput. Geotech. 30 (6), 535–547.
Gatmiri, B., 1992. Response of cross-anisotropic seabed to ocean waves. Journal of Geotechnical Engineering 118 (9), 1295–1314.
Goff, J.A., Kraft, B.J., Mayer, L.A., Schock, S.G., Sommerfield, C.K., Olson, H.C., Gulick, S.P.S., Nordfjord, S., 2004. Seabed characterization on the New Jersey middle and outer shelf: correlatability and spatial variability of seafloor sediment properties. Mar. Geol. 209 (1–4), 147–172.
Goff, J.A., Jenkins, C.J., Williams, S.J., 2008. Seabed mapping and characterization of sediment variability using the usSEABED data base. Cont. Shelf Res. 28 (4–5), 614–633.
Goovaerts, P., 1997. Geostatistics for Natural Resources Evaluation. Oxford university press.
Grasso, S., Maugeri, M., Motta, E., 2012. Site characterisation by in situ and laboratory tests of the sea bed in the Genova Harbour, Italy. Electrical Measuring Instruments and Measurements 415.
Griffiths, D.V., Fenton, G.A., 2001. Bearing capacity of spatially random soil: the undrained clay Prandtl problem revisited. Geotechnique 51 (4), 351–360.
Griffiths, D.V., Fenton, G.A., Manoharan, N., 2002. Bearing capacity of rough rigid strip footing on cohesive soil: probabilistic study. J. Geotech. Geoenviron. Eng. 128 (9), 743–755.
Hsu, J.R.C., Jeng, D.S., Lee, C.P., 1995. Oscillatory soil response and liquefaction in an unsaturated layered seabed. Int. J. Numer. Anal. Methods GeoMech. 19 (12), 825–849.
Jeng, D.S., 1997. Soil response in cross-anisotropic seabed due to standing waves. J. Geotech. Geoenviron. Eng. 123 (1), 9–19.
Jeng, D.S., 2001. Numerical modeling for wave–seabed–pipe interaction in a non-homogeneous porous seabed. Soil Dynam. Earthq. Eng. 21 (8), 699–712.
Jeng, D.S., 2012. Porous Models for Wave-Seabed Interactions. Springer Science & Business Media.
Jeng, D.S., Cheng, L., 1999. Wave-induced seabed response around a pipe laid on a poro-elastic seabed. J. Offshore Mech. Arctic Eng. 121 (4), 227–236.
Jeng, D.S., Cheng, L., 2000. Wave-induced seabed instability around a buried pipeline in a poro-elastic seabed. Ocean. Eng. 27 (2), 127–146.
Jeng, D.S., Lin, Y., 1999. Pore pressure on a submarine pipeline in a cross-anisotropic nonhomogeneous seabed under water-wave loading. Can. Geotech. J. 36 (3), 563–572.
Jeng, D.S., Lin, Y., 2000a. Poroelastic analysis of the wave–seabed interaction problem. Comput. Geotech. 26 (1), 43–64.
Jeng, D.S., Lin, Y., 2000b. Response of inhomogeneous seabed around buried pipeline under ocean waves. J. Eng. Mech. 126 (4), 321–332.
Jeng, D.S., Seymour, B.R., 1997. Response in seabed of finite depth with variable permeability. J. Geotech. Geoenviron. Eng. 123 (10), 902–911.
Jeng, D.S., Postma, P., Lin, Y., 2001. Stresses and deformation of buried pipeline under wave loading. J. Transport. Eng. 127 (5), 398–407.
Jiang, S., Li, D., Cao, Z., Zhou, C., Phoon, K., 2014. Efficient system reliability analysis of slope stability in spatially variable soils using Monte Carlo simulation. J. Geotech. Geoenviron. Eng. 141 (2), 04014096.
Kitano, T., Mase, H., 1999. Boundary-layer theory for anisotropic seabed response to sea waves. J. Waterw. Port, Coast. Ocean Eng. 125 (4), 187–194.
Liu, W., Chen, Q., Wang, C., Juang, C.H., Chen, G., 2017. Spatially correlated multiscale Vs30 mapping and a case study of the Suzhou site. Eng. Geol. 220, 110–122.
Lloret-Cabot, M., Fenton, G.A., Hicks, M.A., 2014. On the estimation of scale of fluctuation in geostatistics. Georisk Assess. Manag. Risk Eng. Syst. Geohazards 8 (2), 129–140.
Magda, W., 1997. Wave-induced uplift force on a submarine pipeline buried in a compressible seabed. Ocean. Eng. 24 (6), 551–576.
Peng, X., Zhang, L., Jeng, D.S., Chen, L., Liao, C., Yang, H., 2017. Effects of cross-correlated multiple spatially random soil properties on wave-induced oscillatory seabed response. Appl. Ocean Res. 62, 57–69.
Phoon, K., Kulhawy, F.H., 1999a. Evaluation of geotechnical property variability. Can. Geotech. J. 36 (4), 625–639.
Phoon, K.K., Kulhawy, F.H., 1999b. Characterization of geotechnical variability. Can. Geotech. J. 36 (4), 612–624.
Rajani, B., Zhan, C., Kuraoka, S., 1996. Pipe soil interaction analysis of jointed water mains. Can. Geotech. J. 33 (3), 393–404.
Rehfeldt, K.R., Boggs, J.M., Gelhar, L.W., 1992. Field study of dispersion in a heterogeneous aquifer: 3. geostatistical analysis of hydraulic conductivity. Water Resour. Res. 28 (12), 3309–3324.
Schock, S.G., 2004. A method for estimating the physical and acoustic properties of the sea bed using chirp sonar data. IEEE J. Ocean. Eng. 29 (4), 1200–1217.
Seymour, B.R., Jeng, D.S., Hsu, J.R.C., 1996. Transient soil response in a porous seabed with variable permeability. Ocean. Eng. 23 (1), 27–46.
Shen, S., Wang, J., Wu, H., Xu, Y., Ye, G., Yin, Z., 2015. Evaluation of hydraulic conductivity for both marine and deltaic deposits based on piezocone testing. Ocean. Eng. 110, 174–182.
Trevorrow, M.V., Yamamoto, T., 1991. Summary of marine sedimentary shear modulus and acoustic speed profile results using a gravity wave inversion technique. J. Acoust. Soc. Am. 90 (1), 441–456.
Tsui, Y., Helfrich, S.C., 1983. Wave-induced pore pressures in submerged sand layer. Journal of Geotechnical Engineering 109 (4), 603–618.
Turcotte, B.R., Liu, P.L.-F., Kulhawy, F.H., 1984. Laboratory Evaluation of Wave Tank Parameters for Wave-Sediment Interaction. Joseph H. Defrees Hydraulic Laboratory Report 84-1, School of Civil and Environmental Engineering. Cornell University.
Ulker, M.B.C., 2012. Pore pressure, stress distributions, and instantaneous liquefaction of two-layer soil under waves. J. Waterw. Port, Coast. Ocean Eng. 138 (6), 435–450.
Valdez-Llamas, Y.P., Auvinet, G., Núñez, J., 2003. Spatial variability of the marine soil in the Gulf of Mexico. In: Offshore Technology Conference. Offshore Technology Conference.
Veloso, F., Navarrete, R., Soria, A., Meléndez, N., 2016. Sedimentary heterogeneity and petrophysical characterization of Barremian tsunami and barrier island/inlet deposits: the Aliaga outcrop as a reservoir analogue (Galve sub-basin, eastern Spain). Mar. Petrol. Geol. 73, 188–211.
Wang, C., Chen, Q., 2017. A hybrid geotechnical and geological data-based framework for multiscale regional liquefaction hazard mapping. Geotechnique 68 (7), 614–625.
Wang, X., Jeng, D.S., Lin, Y., 2000. Effects of a cover layer on wave-induced pore pressure around a buried pipe in an anisotropic seabed. Ocean. Eng. 27 (8), 823–839.
Wang, C., Chen, Q., Shen, M., Juang, C.H., 2017. On the spatial variability of CPT-based geotechnical parameters for regional liquefaction evaluation. Soil Dynam. Earthq. Eng. 95, 153–166.
Wu, H., Shen, S., Ma, L., Yin, Z., Horpibulsuk, S., 2015. Evaluation of the strength increase of marine clay under staged embankment loading: a case study. Mar. Georesour. Geotechnol. 33 (6), 532–541.
Yamamoto, T., Suzuki, Y., 1980. Stability analysis of seafloor foundations. In: Coastal Engineering 1980, pp. 1799–1818.
Yamamoto, T., Torii, T., 1986. Seabed shear modulus profile inversion using surface gravity (water) wave-induced bottom motion. Geophys. J. Int. 85 (2), 413–431.
Ye, J., 2012. 3D liquefaction criteria for seabed considering the cohesion and friction of soil. Appl. Ocean Res. 37, 111–119.
Zen, K., Yamazaki, H., 1990a. Mechanism of wave-induced liquefaction and densification in seabed. Soils Found. 30 (4), 90–104.
Zen, K., Yamazaki, H., 1990b. Oscillatory pore pressure and liquefaction in seabed induced by ocean waves. Soils Found. 30 (4), 147–161.
Zhang, L., Zhang, L., Tang, W., 2004. Rainfall-induced slope failure considering variability of soil properties. Geotechnique 55 (2), 183–188.
Zhang, L., Cheng, Y., Li, J., Zhou, X., Jeng, D.S., Peng, X., 2016. Wave-induced oscillatory response in a randomly heterogeneous porous seabed. Ocean. Eng. 111, 116–127.
Zhao, H., Jeng, D.S., Liao, C., 2016a. Parametric study of the wave-induced residual liquefaction around an embedded pipeline. Appl. Ocean Res. 55, 163–180.
Zhao, H., Jeng, D.S., Liao, C., 2016b. Effects of cross-anisotropic soil behaviour on the

wave-induced residual liquefaction in the vicinity of pipeline buried in elasto-plastic seabed foundations. Soil Dynam. Earthq. Eng. 80, 40–55.
Zhou, X., Xu, B., Wang, J., Li, Y., 2011. An analytical solution for wave-induced seabed response in a multi-layered poro-elastic seabed. Ocean. Eng. 38 (1), 119–129.
Zhou, X., Jeng, D.S., Yan, Y., Wang, J., 2013. Wave-induced multi-layered seabed response around a buried pipeline. Ocean. Eng. 72, 195–208.
Zhou, X., Wang, J.H., Zhang, J., Jeng, D.S., 2014. Wave and current induced seabed response around a submarine pipeline in an anisotropic seabed. Ocean. Eng. 75, 112–127.